# Molecular simulation of static hyper-Rayleigh scattering : a calculation of the depolarization ratio and the local fields for liquid nitrobenzene

# Molecular simulation of static hyper-Rayleigh scattering: A calculation of the depolarization ratio and the local fields for liquid nitrobenzene

R. H. C. Janssen[a] and D. N. Theodorou[b]
*Department of Chemical Engineering, University of Patras and Institute of Chemical Engineering and High Temperature Chemical Processes, GR 26500 Patras, Greece*

S. Raptis[c] and M. G. Papadopoulos
*Institute of Organic and Pharmaceutical Chemistry, National Hellenic Research Foundation, Vassileos Constantinou 48, GR 11635 Athens, Greece*

(Received 5 March 1999; accepted 24 August 1999)

Molecular dynamics (MD) simulation is used to assess the hyper-Rayleigh scattering (HRS) depolarization ratio of liquid nitrobenzene subject to vertically polarized light. In contrast to previous theoretical work, we have quantified both incoherent *and* coherent scattering arising from positional and orientational inhomogeneities in the molecular distribution. Although coherent scattering is shown to be much less important than in the case of Rayleigh scattering, it can not be neglected. Therefore, our analysis supports the current practice of working with dilute solutions (for which coherent contributions to HRS are truly negligible) to extract the first molecular hyperpolarizability from HRS measurements. In cases where experiments with pure liquids can not be circumvented, our analysis may be used to separate coherent and incoherent signals. Our work, which uses as input static ''gas-phase'' (hyper)polarizabilities obtained from *ab initio* calculations, also provides information on the orientations and magnitudes of the local electric fields experienced by the individual molecules in the liquid. For nitrobenzene it is found that the local fields are largely determined by specific dipolar alignment between neighboring pairs of molecules, with consequences on the HRS signal. © *1999 American Institute of Physics.*
[S0021-9606(99)51143-4]

## I. INTRODUCTION

A molecular liquid irradiated by a laser of frequency $\omega$ scatters a small fraction of the incident power in the form of light at the same frequency $\omega$. This is known as Rayleigh scattering. A much smaller fraction of incident power is scattered as light at the second harmonic frequency $2\omega$. This hyper-Rayleigh scattering (HRS) is only noticeable upon intense irradiation of the liquid. (Typically intensities of 10 GW/cm$^2$ are used, corresponding to an external field of approximately $10^8$ V/m.) HRS arises from the nonlinear response of the molecules to intense electromagnetic (EM) fields [see, e.g., Refs. 1 and 2 and Eq. (1) of this paper]. In recent years it has become apparent that measurement of HRS in liquids may be used to quantify the nonlinearity in the molecular response: Clays and Persoons[3,4] have shown that measurement of HRS signals allows extracting reliable values for the largest element of the molecular first hyperpolarizability tensor $\beta_{ijk}$ [with $i,j,k \in \{x,y,z\}$, and $(x,y,z)$ denoting the *molecular* coordinate frame]. Furthermore, subsequent experimental[5] and theoretical[6] work has indicated that the HRS-technique may also be used to determine the values of the other elements of the molecular $\beta_{ijk}$ tensor, essentially by measuring HRS-depolarization ratios in a series of experiments utilizing both linearly and circularly polarized light.[7] As a result, HRS, first observed in the 1960s,[8] nowadays has developed into an important tool in the nonlinear optics (NLO) field.

Whereas the objective of most experimental work on HRS has been the determination of the (elements of the) molecular hyperpolarizability from macroscopic observables (such as the depolarization ratio or scattered intensities), our goal is opposite and complementary: Using molecular simulation, we wish to calculate the depolarization ratio of liquid nitrobenzene subject to a *Z*-polarized incident beam propagating in the *X* direction, using as input high quality molecular (hyper)polarizabilities obtained from *ab initio* quantum mechanical calculations. [We use $(X,Y,Z)$ to denote the *laboratory* coordinate frame.] In doing so we aim at quantifying both incoherent and coherent contributions to the hyper-Rayleigh scattering signal.[9–11] As far as we are aware, our calculation is the first to produce precise estimates of the importance of the coherent contribution to the HRS signals. Moreover, our work allows to assess in detail the magnitudes and orientations of the local fields experienced by the molecules.

The current contribution is part of a wider effort aiming at establishing quantitative relations between molecular and material properties of disordered substances. Recently, we have developed a combined molecular dynamics/

[a]Present address: Department of Chemical Engineering, Eindhoven University of Technology, P.O. Box 513, 5600 MB Eindhoven, The Netherlands.
[b]Author to whom correspondence should be addressed at the University of Patras. Tel: +3061997398; Fax: +3061993255; electronic mail: doros@sequoia.chemeng.upatras.gr
[c]Also at Chemical Engineering Department, National Technical University of Athens, Zografou Campus, Athens 15773, Greece.

 

electrostatics method[12] that does not invoke the use of local field factors, but instead directly calculates the local electric fields experienced by a representative sample of molecules in a liquid. Our method of ''*a posteriori*'' application of an external field to equilibrium liquid configurations is also used in the current contribution. Its details are as described in Ref. 12. Therefore, in the next section we briefly recapitulate our approach and focus attention on new aspects.

The outline of the rest of the paper is as follows. In Sec. II we present the theoretical considerations of concern in the current problem, briefly review the computational strategy (Sec. II A), and give an overview of all molecular data (Sec. II B). Section III presents our results on structure and dynamics of the liquid (Sec. III A), orientation and magnitude of local fields (Sec. III B), and the HRS-depolarization ratio (Sec. III C). Conclusions are drawn in the final Sec. IV.

## II. THEORETICAL CONSIDERATIONS

Each molecule $i$ in a macroscopic amount of liquid experiences a local electric field $\underline{E}_{\mathrm{loc},i}$ that induces a dipole moment in the molecule given by[13]

$$\underline{\mu}_{\mathrm{ind},i} = \underline{\underline{\alpha}} \cdot \underline{E}_{\mathrm{loc},i} + \underline{\underline{\underline{\beta}}} : \underline{EE}_{\mathrm{loc},i} + \cdots . \tag{1}$$

In this equation, $\underline{EE}_{\mathrm{loc},i}$ is a 2nd order tensor formed from $\underline{E}_{\mathrm{loc},i}$, denoting the nonlinear contribution to $\underline{\mu}_{\mathrm{ind},i}$. The $\underline{\underline{\alpha}}$ and $\underline{\underline{\underline{\beta}}}$ are the molecular polarizability and first hyperpolarizability tensors, with elements $\alpha_{ij}$ and $\beta_{ijk}$. The values of the elements are determined by the properties of the molecule, but may also depend on the frequency of $\underline{E}_{\mathrm{loc},i}$.[1,2]

Based on the dipole oscillator expression, as known from classical electromagnetism,[14] the average intensity of the HRS signal generated by a $Z$-polarized incident beam propagating along the $X$-axis can be written as[5,7,8]

$$I_J^{2\omega} \sim \frac{(2\omega)^4}{32\pi^2 \epsilon_0 c^4 r^2} \left\langle \sum_{k=1}^{N} \sum_{l=1}^{N} \mu_{\beta,kJ} \mu_{\beta,lJ} e^{-i\underline{k}\cdot\underline{r}_{kl}} \right\rangle \tag{2}$$

in which we use $\sim$ to indicate that $I_J^{2\omega}$ has units of energy density J/m$^3$. Conversion to real intensity units, J/(m$^2$s), is straightforward by multiplying with $c/n$, $c$ being the velocity of light in vacuum and $n$ the refractive index of the material at $2\omega$. We have not made this conversion, since we are interested in the depolarization ratio $D = I_X^{2\omega}/I_Z^{2\omega}$, for which these prefactors cancel. In Eq. (2), $J$ denotes the $J$-polarized component of the scattered light (we only consider scattered light propagating in the $Y$ direction, so $J \in \{X,Z\}$), $r$ is the average distance of the detector from the center of illumination of the sample, and $\epsilon_0$ is the dielectric permittivity of vacuum. The sums in Eq. (2) run over all molecules in the volume from which the scattering is considered. The $\beta,kJ$ subscript on the induced dipole moment $\mu$ indicates that only the $J$-axis projection of the $\beta$ term of molecule $k$ is considered [by $\beta$ term we mean the second term on the right-hand side of Eq. (1)]. The exponential factor in Eq. (2) accounts for the angular dependence of the scattered intensity. In the exponent, $r_{kl} = r_k - r_l$ points from scatterer $l$ to scatterer $k$ and the wave vector is defined as $\underline{k} = 4\pi/\lambda \sin(\theta/2)(\underline{u} - \underline{u}_0)$ with $\lambda$ the wavelength of the incident beam, $\theta$ the scattering angle, and $\underline{u}, \underline{u}_0$ unit vectors in the direction of the scattered and incident radiation.[9] Finally, the brackets in Eq. (2) denote time averaging over many liquid configurations subject to an external field.

The scattering signal of Eq. (2) contains an interference-free incoherent contribution due to single molecules (obtained for $k=l$), and a coherent contribution arising from inhomogeneities in the spatial and orientational distribution of the molecules within the medium (obtained for $k \neq l$). In principle, the coherent scattering is subject to interference effects arising from the angular dependence that occurs when $k \neq l$ [note from Eq. (2) that the angular dependence vanishes for $k=l$, i.e., for incoherent scattering]. However, for (hyper-)Rayleigh scattering this angular dependence virtually absent. In Rayleigh scattering, for which an expression identical to Eq. (2) can be written,[9–11] this is due to vanishing of correlations in molecular packing over distances $r_{kl} \ll \lambda$. Then, $\underline{k} \cdot \underline{r}_{kl} \to 0$ and $e^{-i\underline{k}\cdot\underline{r}_{kl}} \to 1$, leaving no $\theta$ dependence. For HRS an identical argument holds:[7] The occurrence of coherent HRS requires both density fluctuations (as does Rayleigh scattering) *and* correlations in molecular orientation,[7] creating locally a noncentrosymmetric molecular environment. The combined density–orientational fluctuations persist over smaller distances than density fluctuations alone and therefore, in HRS scattering, as in Rayleigh scattering, the exponential factor appearing in Eq. (2) may be taken as 1.

Since coherent HRS is promoted by molecular correlations that persist over smaller distances than in Rayleigh scattering,[7] its contribution to the total scattering signal is also expected to be smaller than in Rayleigh scattering.[3–7] However, as far as we are aware, the precise balance between coherent and incoherent HRS has never been estimated for any substance. In order to fill this gap, we have taken up this task for liquid nitrobenzene. Our procedure is briefly sketched in Sec. II A.

Here we need to address two more aspects of Eq. (2). First, Eq. (2) only accounts for *static* HRS. Peak broadening[8] of the HRS signal due to molecular motion is not taken into account, although this can in principle be done via MD methods (see Refs. 9, 15, and 16 for examples dealing with Rayleigh scattering). Secondly, we need to clearly discuss the limitations of Eq. (2). Generally, in an actual experiment, the volume from which scattering originates has dimensions that are commensurate with the wavelength $\lambda \sim 7500$ Å of the incident beam. However, our MD simulation can only treat volumes $L^3$ with $L$ on the order of 10 Å containing at maximum a few hundred molecules. As a consequence, MD simulation can not be used directly to study (multiple) scattering processes responsible for attenuation of the incident beam upon traversing a sample,[10] and it can not incorporate in a straightforward manner cooperative effects among induced dipoles separated by distances larger that the box length $L$. To treat the last problem, we think of the fluid as a periodic array of boxes (volume elements), each containing an exact copy of the contents of the ''parent'' box, and use the Ewald summation technique[17,18] to extend the electrostatic interactions to an infinitely large volume. In contrast, attenuation of the incident beam upon traversing the sample is not accounted for: It is assumed that every volume element

is subject to the same externally imposed field and that the electronic responses to the field are instantaneous. This assumption is reasonable when the scattered intensities are weak in comparison with the intensity of the incident radiation,[19] which is indeed the case for (hyper-)Rayleigh scattering. We believe that our approach provides an interesting alternative to immersing the simulation box in a dielectric continuum:[10] It does not need as input macroscopic susceptibilities of the surrounding dielectric (refractive index or nonlinear susceptibilities), and therefore does not require the self-consistent determination of these quantities from molecular simulation.

### A. Computational strategy

In this section we briefly recapitulate our method to obtain the $\underline{E}_{\mathrm{loc},i}$, first presented in Ref. 12. Our strategy relies on a two step process.

In step 1, a liquid at ambient density $\rho = 9.763 \times 10^3$ mole/m$^3$ and temperature $T = 298$ K is simulated in a fully equilibrated 850 ps microcanonical[9] constraint[20,21] MD of 72 nitrobenzene molecules in a cubic box with edge $L = 23.05$ Å subject to periodic boundary conditions.[22] A total of 8500 liquid configurations are collected by saving consecutive configurations every 0.1 ps. In the MD no external field is present, we simply perform an equilibrium simulation.

After the simulation, in step 2, each liquid configuration is placed in an electric field $\underline{E} = (0,0,E_Z)$, representing a $Z$-polarized laser beam, and a point-polarizable dipole is allowed to be developed at the center of the phenyl ring of each molecule. The $\underline{E}_{\mathrm{loc},i}$, consisting of a sum of the external field $E$ and the fields due to the permanent and induced dipoles of the nitrobenzene molecules, can now be obtained by iteratively solving the electrostatics problem[12] constituted by Eq. (1) of this paper and Eqs. (17)–(19) of Ref. 12 [Eqs. (17)–(19) provide expressions for the sum of the dipolar fields of the molecules]. Our method is essentially identical to methods developed in the 1970's to access the optical properties of crystals[23] and does not invoke the commonly employed local field factors.[1,24] Note that we only assign one dipole to each molecule. In a first approximation this is sufficient, as was shown by similar calculations on low-molecular crystalline materials, such as urea and benzene, by varying the number of dipoles to be developed in each molecule (see Ref. 23 and references cited therein). Once $\underline{E}_{\mathrm{loc},i}$ is known for each molecule in every liquid configuration, the $I_X^{2\omega}$, $I_Z^{2\omega}$, and $D$ are found from Eqs. (1) and (2). It should be realized that the average in Eq. (2) is a field-on average. Therefore, as explained in Ref. 12, it is necessary to reweight the configurations generated in the (equilibrium) MD by a factor $\exp(V\underline{\mathcal{P}}_{\mathrm{ind}} \cdot \underline{E}/k_B T)$, in which $\underline{\mathcal{P}}_{\mathrm{ind}}$ is the electronic polarization induced by the externally applied field. However, for fields $\underline{E} \leqslant 10^9$ V/m, the exponent does not significantly differ from 1 in weakly nonlinear substances such as nitrobenzene.[12] Thus, we may simply take the equilibrium average generated in the MD. Physically, this amounts to assuming that the optical field has no influence on the liquid structure, which is reasonable, since, in a first approximation, an optical field does not alter the organization of molecules, but merely induces dipole moments in them.[24] This procedure of ''*a posteriori*'' application of an external field to equilibrium liquid configurations has previously been employed, e.g., by Ladanyi.[16]

### B. Molecular model

In the simulation an all-atom representation, based on work by Shlyapochnikov *et al.*,[25] was used for nitrobenzene. The molecular model employs fixed bond lengths and angles and uses a bistable torsional potential for the $NO_2$ group that favors planar conformations. The energy barrier of this torsional potential was chosen as 3.0 kcal mole$^{-1}$, in agreement with experimental data.[25] The interatomic interaction potentials were chosen to be of standard Lennard-Jones + partial charge type.[22] The LJ parameters were taken from previous work on benzene,[12] with the parameters for the atoms of the nitro group based on Table 1.1 of Ref. 22. No effort to further optimize the LJ-parameters was made. Atomic partial charges, taken from a Mulliken population analysis, were rescaled to create a molecular dipole moment of 4.36 D, in agreement with experimental values.[24–26] Note that the interparticle potentials do not account for the polarizable nature of the molecules. Sole purpose of the MD was to efficiently generate realistic equilibrium liquid configurations. Molecular (hyper)polarizabilities are only needed in the electrostatics calculations (stage 2). An overview of all molecular data is given in Table I.

The molecular (hyper)polarizability tensors $\underline{\underline{\alpha}}$ and $\underline{\underline{\underline{\beta}}}$ used in the calculation of the $\underline{E}_{\mathrm{loc},i}$ were obtained with the GAMESS package[27] from single molecule static *ab initio* calculations at the MP2 level employing a Sadlej basis set.[28] The $\underline{\underline{\alpha}}$ and $\underline{\underline{\underline{\beta}}}$ were obtained using finite perturbation theory with an electric field of 0.003 a.u. Attempts to account for the effect of the molecule's local environment on the (hyper-)polarizabilities (solvent effect) have not been made and are beyond the scope of the present investigation. The molecular geometry used in the quantum calculations was optimized at the MP2-level[29] using the 6-31G** basis set.[30] In Table I, the values of the nonzero (hyper)polarizability tensor elements are given in atomic units. Conversion to SI units is straightforward (1 a.u. of $\underline{\underline{\alpha}} = 0.164\,867 \times 10^{-40}\,\mathrm{C^2\,m^2\,J^{-1}}$ and 1 a.u. of $\underline{\underline{\underline{\beta}}} = 0.320\,662 \times 10^{-52}\,\mathrm{C^3\,m^3\,J^{-2}}$). The calculated (hyper)polarizability tensor elements lead to orientationally averaged molecular (hyper)polarizabilities of, respectively, $\alpha = \Sigma_i \alpha_{ii} = 88.34$ a.u. and $\beta = 1/3 \Sigma_i (\beta_{zii} + \beta_{izi} + \beta_{iiz}) = -161.6$ a.u. This value of $\beta$ refers to the molecular orientation given in Fig. 1, for which $\mu = \mu_z < 0$ (i.e., the permanent dipole moment is directed along the negative $z$-axis). The $\alpha$ falls within the range of experimental values reported in Refs. 24, 26, and 31. Our computed value for $\beta$ is also in reasonable agreement with that measured experimentally, $\beta = 128 \pm 19.7$ a.u. by Singer and Garito[31] and 235 a.u. by Levine and Bethea.[32]

## III. RESULTS AND DISCUSSION

This section is divided in three parts. In Sec. III A, the structural and dynamical properties of the liquid are presented. In Sec. III B, results are shown for the local fields

TABLE I. Molecular data.

| | |
|---|---|
| Bond lengths (Å): | |
| CC; CH; CN; NO | 1.401; 1.031; 1.459; 1.194 |
| ONO-bond angle (degrees): | 124.6 |
| Atomic charges ($e$):* | |
| C1; C2=C3; | −0.112 71; −0.151 97; |
| C4=C5; C6; | −0.113 94; 0.021 78; |
| N7; O8=O9; | 0.410 70; −0.292 69; |
| H10; H11=H12; | 0.150 75; 0.152 96; |
| H13=H14 | 0.170 38 |
| LJ parameters (kcal mole$^{-1}$ Å$^{12}$; kcal mole$^{-1}$ Å$^{6}$): | |
| $A_{CC}$; $B_{CC}$ | 692 949.3; 547.6 |
| $A_{CH}$; $B_{CH}$ | 88 214.6; 103.7 |
| $A_{HH}$; $B_{HH}$ | 5021.5; 15.82 |
| $A_{CN}$; $B_{CN}$ | 527 203.0; 404.5 |
| $A_{HN}$; $B_{HN}$ | 70 771.6; 86.2 |
| $A_{CO}$; $B_{CO}$ | 548 103.6; 491.7 |
| $A_{HO}$; $B_{HO}$ | 56 866.6; 86.28 |
| $A_{NN}$; $B_{NN}$ | 512 795.2; 389.9 |
| $A_{OO}$; $B_{OO}$ | 335 997.3; 393.6 |
| $A_{NO}$; $B_{NO}$ | 395 029.6; 354.4 |
| Rotational energy barrier (kcal mole$^{-1}$): | 3.0 |
| Polarizability $\underline{\alpha}$ (au): | |
| $\alpha_{xx}$; $\alpha_{yy}$; $\alpha_{zz}$ | 50.90; 98.98; 115.15 |
| First hyperpolarizability $\underline{\beta}$ (au): | |
| $\beta_{xxz}=\beta_{xzx}=\beta_{zxx}$ | 27.4 |
| $\beta_{yyz}=\beta_{yzy}=\beta_{zyy}$ | 4.7 |
| $\beta_{zzz}$ | −193.6 |

[a]Atom numbers and molecular coordinate frame are shown in Fig. 1.

experienced by the nitrobenzene molecules. Finally, in Sec. III C we present and discuss our results on the HRS-depolarization ratio of the liquid.

### A. Liquid structure and dynamics

Figure 2 shows the radial distribution function $g(r)$ for the phenyl centers of the nitrobenzene molecules and Figs. 3 and 4 provide information on the orientational intermolecular correlations within the liquid. Figure 3 depicts the orientational correlation of the permanent dipoles, $P_1(r)$, defined by

$$P_1(r)=\langle \cos \phi_{ij}(r)\rangle \tag{3}$$

with $\phi_{ij}(r)$ the angle between unit vectors directed along the permanent dipoles of molecules $i$ and $j$. Figure 4 shows the orientational correlation of the phenyl rings, $P_2(r)$, defined by

$$P_2(r)=\langle (3\cos^2 \theta_{ij}(r)-1)/2\rangle \tag{4}$$

with $\theta_{ij}(r)$ the angle between unit vectors perpendicular to the phenyl rings of molecules $i$ and $j$. In Eqs. (3) and (4), $r$ is taken as the distance between the centers of the phenyl rings and the angular brackets denote averaging over all configurations and all pairs of molecules at distance $r$. Note that, in constructing Figs. 3 and 4, we have used a first order Legendre polynominal, $P_1(r)$, to analyze dipolar correlations and a second order polynomial to study correlations between the phenyl rings. This is appropriate since dipolar ordering, in contrast to the orientational ordering of the phenyl rings, has a sense of direction.

In Fig. 2, the two peaks in the radial distribution function for $r=3.9$ Å and $r=5.2$ Å correspond to nearest neighbor arrangements of the nitrobenzene molecules. Together, they

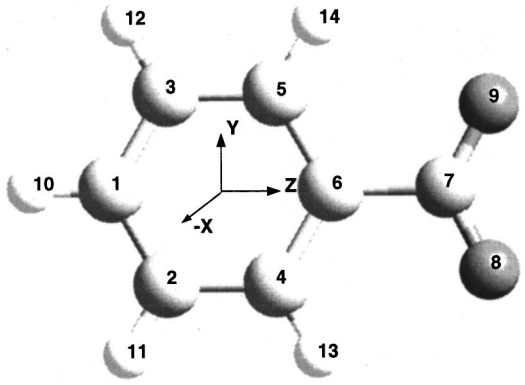


FIG. 1. Atom numbers and molecular coordinate frame of the nitrobenzene molecule. The positive molecular $x$-axis points into the paper.

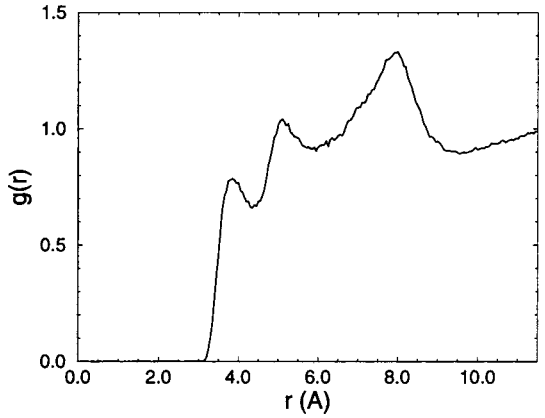


FIG. 2. Radial distribution function of phenyl ring centers in liquid nitrobenzene.

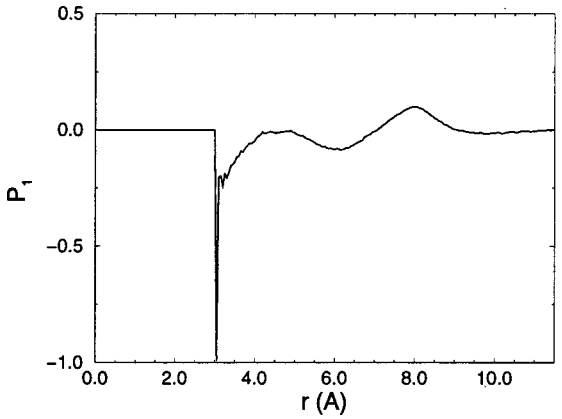


FIG. 3. Orientational correlation function of permanent dipole moments in liquid nitrobenzene.

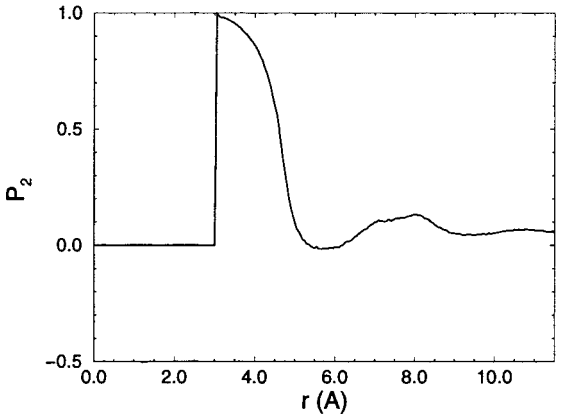


FIG. 4. Orientational correlation function of phenyl rings in liquid nitrobenzene.

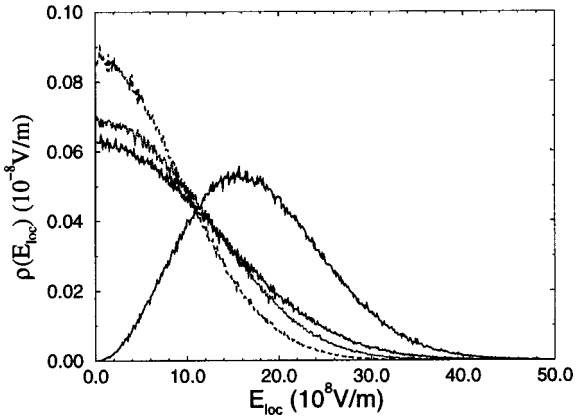


FIG. 5. Normalized distribution of electric field strengths experienced by phenyl centers. The curve displaying a maximum represents the distribution of magnitudes of the local field vector, while the other curves depict the magnitudes of local field components monitored along the molecular *y*-axis (upper line on left-hand side of the figure), *x*-axis (lower line), and *z*-axis.

constitute the first coordination shell. As is clearly seen from Figs. 2–4, in the region 3 Å–4.5 Å, i.e., in the vicinity of the first correlation peak, the permanent dipoles of the molecular pairs tend to be aligned antiparallel to each other (negative $P_1$, Fig. 3), whereas the phenyl rings are oriented parallel (Fig. 4). In the region around the second peak in the first coordination shell, i.e., around $r=5.2$ Å, the orientational ordering of the nitrobenzene molecules is much less pronounced (see Figs. 3 and 4). Thus, Figs. 2–4 indicate that within the first correlation shell, molecular pairs with a strong, nevertheless not perfect, tendency for antiparallel alignment are formed (note that this tendency is larger for smaller intermolecular distances). This aspect of the intermolecular packing is in good agreement with previous work by Piekara and Chelkowski who proposed on the basis of the anomalous positive nonlinear dielectric saturation observed in liquid nitrobenzene, that part of the nitrobenzene molecules order into dimers with a nearly antiparallel dipolar coupling.[33,34]

The second correlation shell of $g(r)$, centered around 8 Å, is broad and contains a relatively large variety of molecular arrangements. The peak itself may be attributed to a stacking of three molecules with antiparallel dipolar ordering. Such a packing is supported by Figs. 3 and 4 in which $P_1>0$ and $P_2>0$ around $r=8$ Å.

Unfortunately, we have not found experimental evidence in the form of x-ray data that may support Figs. 2–4. Nevertheless, the figures are shown since they support the concept of dimerization as introduced by Piekara,[34] and more importantly, since they clearly indicate that the correlations in packing (Fig. 2) and orientation (Figs. 3 and 4) have largely vanished beyond $r=10$ Å. This implies that the box size is large enough to ensure vanishing of density and orientational fluctuations on length scales smaller than the box size. As indicated in Sec. II, this guarantees that coherent HRS will only be produced from molecular pairs located within the simulation box and minimizes the influence of the periodic boundaries on the HRS-depolarization ratio, for which results will be presented in Sec. III C.

The dynamical properties of our model liquid are as follows. The self-diffusivity from the mean squared displacement of the molecular centers of mass was found to be 0.4 $\times 10^{-5}$ cm$^2$/s, in reasonable agreement with experimental values.[35] Furthermore, we have observed infrequent torsional transitions of the nitro group by 180° around the molecular C–N bond with a time constant of approximately 120 ps.

### B. Local fields

The main results obtained for the local fields $\underline{E}_{\mathrm{loc},i}$ experienced by the phenyl ring centers in a liquid not subjected to an external field are shown in Figs. 5–8. These results were obtained by directly solving for each liquid configuration the electrostatics problem given by Eq. (1) of this work and Eqs. (17)–(19) of Ref. 12. No local field factors were used.

Figure 5 depicts the distribution of local field strengths monitored along the molecular axes (axes are defined in Fig. 1). The figure also shows the distribution of the magnitude of the local field strength defined by $E_{\mathrm{loc}}=\sqrt{E_{\mathrm{loc},x}^2+E_{\mathrm{loc},y}^2+E_{\mathrm{loc},z}^2}$. The magnitude is skewed towards

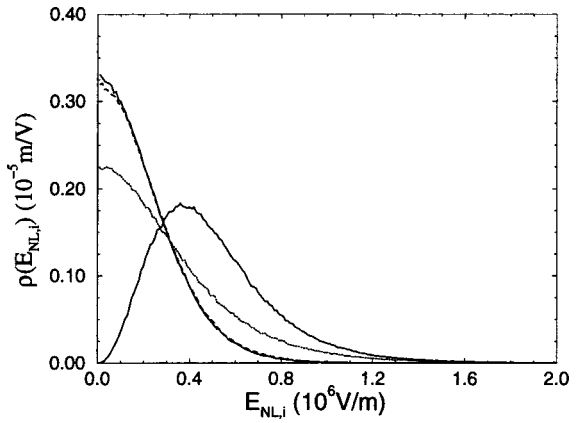


FIG. 6. Normalized distribution of the explicit nonlinear contributions to the local fields experienced by the phenyl rings. The curve displaying a maximum represents the magnitudes of the total nonlinear contribution to the local fields. The other curves represent the nonlinear contributions monitored along the molecular *x*- and *y*-axis (upper curves on left-hand side of the figure) and the contribution monitored along the *z*-axis (lower curve). Note that the nonlinear field strengths along the *x*- and *y*-axis are roughly equal.

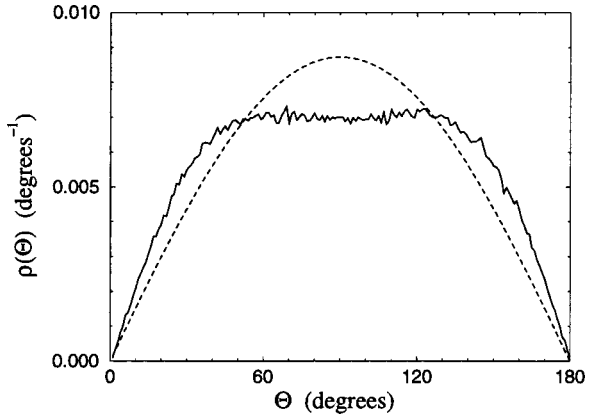


FIG. 7. Normalized orientational distribution of the local fields with respect to the molecular *x*-axis. $\theta=90°$ corresponds to a field in the plane of the phenyl ring. The dashed curve denotes the distribution corresponding to the case of no directional preference with respect to the *x*-axis.

large $E$ with a peak value at $E_{\mathrm{loc}}=1.7\times10^9$ V/m. This value is higher than $1.3\times10^9$ V/m found in liquid benzene,[12] as expected from the dipolar nature of the nitrobenzene liquid, but lower than $4.2\times10^9$ V/m obtained by a classical reaction field (RF) analysis on nitrobenzene (see Chap. 3 of Ref. 24). The discrepancy with the RF approach is not very surprising, since the latter approach should merely be regarded as an order of magnitude estimation, whereas our method provides more detailed information on the local molecular environment. From Fig. 5 it is also seen that the fields in the molecular *z* direction tend to assume higher values than in the *y* direction, which can be explained by the fact that the dipole moment is directed along the negative *z*-axis (see Table I): A dipole along the negative molecular *z*-axis results in a strong parallel reaction field produced by the surrounding molecules. Interestingly, perpendicular to the phenyl ring along the molecular *x*-axis approximately the same field strengths are monitored as along the *z*-axis. This is due to the specific way many neighboring molecules are arranged: It is easy to envisage that neighboring molecules with a strong tendency for antiparallel dipolar alignment (as is the case for the molecular pairs with the closest separation distances, see Figs. 2–4) produce strong $E_{\mathrm{loc},x}$ fields perpendicular to the rings (especially since the intermolecular distance is very short in the *x* direction). Clearly, the arrangement of these pairs does not lead to large $E_{\mathrm{loc},y}$ fields. In contrast, the more or less random arrangement of dipoles around $r=5.2$ Å, in the second peak of the first correlation shell, produces weaker fields along both the *x*- and *y*-axes of the molecules (*weaker*, because for these pairs the intermolecular separation distances are larger).

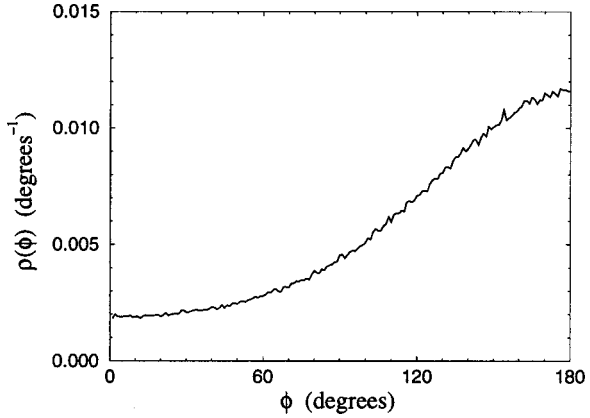


FIG. 8. Normalized orientational distribution of the in-plane projection of the local field vector with respect to the molecular *z*-axis. $\phi=180°$ corresponds to an in-plane field parallel to the molecular dipole moment.

Obviously, the field strengths monitored along the axes are influenced by the anisotropic shape of the nitrobenzene molecule. To study this we have used the configurations generated in the MD run to go through a separate electrostatics calculation on ''nitrobenzene'' without a permanent dipole moment (using the same partial charges as in benzene[12]) and with isotropic (hyper)polarizabilities. In this case, we found much smaller differences between the local field components, the order $|E_{\mathrm{loc},x}|\geqslant|E_{\mathrm{loc},y}|\geqslant|E_{\mathrm{loc},z}|$ being determined by the molecular shape. Based on the large difference between the results of the two calculations, we conclude that antiparallel dipolar alignment and not molecular shape is most important in determining the local fields.

In Fig. 6, explicit nonlinear contributions to the molecular fields are isolated. Both the distributions of the nonlinear contributions monitored along the axes of the phenyl ring and the magnitude of the total nonlinear contribution, determined from $E_{\mathrm{loc,NL}}=\sqrt{E^2_{\mathrm{loc},x,\mathrm{NL}}+E^2_{\mathrm{loc},y,\mathrm{NL}}+E^2_{\mathrm{loc},z,\mathrm{NL}}}$, are given. Figure 6 shows that the highest value of $E_{\mathrm{loc,NL}}$ is monitored along the molecular *z*-axis, as expected from $|\beta_{zzz}|>>>|\beta_{xxx}|$, $|\beta_{yyy}|$ (see Table I). Furthermore, the magnitude of $E_{\mathrm{loc,NL}}$ like the magnitude of $E_{\mathrm{loc}}$, is skewed towards large fields. By comparing Figs. 5 and 6 it is also apparent that the peak value of $E_{\mathrm{loc,NL}}$ located around $\sim4\times10^5$ V/m is negligible when compared to the peak in the total field strength $\sim1.7\times10^9$ V/m. Therefore, liquid nitrobenzene is only a weakly nonlinear substance, whose electrostatics in the absence of a strong external field can be fully quantified in terms of a linear polarizability $\underline{\underline{\alpha}}$. By comparing Fig. 6 to Fig. 3 of Ref. 12 it is seen that the magnitude of the nonlinear contribution to the local fields in nitrobenzene is only by a factor 3 larger than in liquid benzene (which is an extremely linear substance). This also follows directly from $|\underline{\underline{\underline{\beta}}}:\underline{EE}_{\mathrm{loc,nitrobenzene}}|\approx3|\underline{\underline{\underline{\gamma}}}:\underline{EEE}_{\mathrm{loc,benzene}}|$. Note that we have not studied the influence of higher order molecular tensors on the strengths of the nonlinear parts of the local fields. Although including a $\underline{\underline{\underline{\gamma}}}$ tensor in Eq. (1) is expected to have some influence on the $\underline{E}_{\mathrm{loc,NL}}$, its effects have not been investigated in view of the uncertainties already present in the current level of description (i.e., in the experimental[31,32] and quantum-mechanical $\underline{\underline{\underline{\beta}}}$ tensor).

In Fig. 7, the distribution of the angle of $\underline{E}_{\mathrm{loc},i}$ with the molecular *x*-axis is shown ($\theta=0°$ corresponds to alignment of $\underline{E}_{\mathrm{loc},i}$ with the positive *x*-axis). The dashed line indicates the distribution that would have been obtained if there had been no directional preference of $\underline{E}_{\mathrm{loc},i}$. Clearly, the local field vector tends to be tilted out of the plane of the phenyl ring. This is consistent with the large magnitude of the out-of-plane component $E_{\mathrm{loc},x}$ seen in Fig. 5. Local fields $\underline{E}_{\mathrm{loc},i}$ perfectly perpendicular to the phenyl ring are scarce (Fig. 7),

TABLE II. Depolarization ratios[a] and scattered intensities.[b]

| | Simulation | Other work |
|---|---|---|
| $I^{2\omega}_{X,\mathrm{incoh}}$; $I^{2\omega}_{X,\mathrm{coh}}$ | 0.046; 0.044 | |
| $I^{2\omega}_{Z,\mathrm{incoh}}$; $I^{2\omega}_{Z,\mathrm{coh}}$ | 0.166; 0.147 | |
| $D_{\mathrm{incoh}}$ | 0.28 | 0.275[c] |
| $D$ | 0.29 | |
| $I^{\omega}_{X,\mathrm{incoh}}$; $I^{\omega}_{X,\mathrm{coh}}$ | 0.02; 0.107 | |
| $I^{\omega}_{Z,\mathrm{incoh}}$; $I^{\omega}_{Z,\mathrm{coh}}$ | 0.690; 47.86 | |
| $\Delta_{\mathrm{incoh}}$ | 0.03 | 0.029[d] |
| $\Delta$ | 0.003 | |

[a]$\Delta$, $\Delta_{\mathrm{incoh}}$, $D$ and $D_{\mathrm{incoh}}$ are accurate within 5%. Error estimates were obtained by applying external fields along different axes of the simulation box.
[b]Scattered intensities are given in arbitrary units and are accurate within 2.5%. In order to relate $I^{\omega}_{J}$ and $I^{2\omega}_{J}$ on an absolute scale, one has to multiply the $I^{2\omega}_{J}$ by $10^{-7}$.
[c]Calculated according to Eq. (6).
[d]Calculated according to Eq. (5).

because large $E_{\mathrm{loc},x}$ are usually accompanied by large $E_{\mathrm{loc},z}$. As already stated, this is indeed the case for neighboring molecules that pack in an antiparallel dipolar fashion.

In Fig. 8, the angular distribution of the in-plane projection of the local field vector with the positive $z$-axis is shown ($\phi=0°$ corresponds to alignment of the in-plane projection with the positive $z$-axis). Figure 8 clearly shows that the in-plane projection of the local field vector tends to point along the permanent dipole, in the negative $z$ direction.

### C. HRS-depolarization ratio

Generally, it is known that coherent scattering mechanisms are less important in hyper-Rayleigh scattering than in Rayleigh scattering.[7] However, up to now, no numbers quantifying the balance between coherent and incoherent HRS radiation have been available. The purpose of the work presented in this section was to fill this gap for the case of liquid nitrobenzene. Static Rayleigh scattering is also treated to get a frame of reference and to focus attention on the differences with HRS.

Our results were obtained by applying to each liquid configuration an external field $\underline{E}=(0,0,E_Z)$ with $E_Z=10^8$ V/m and solving for $\underline{E}_{\mathrm{loc},i}$ according to the scheme of Ref. 12. Once the $\underline{E}_{\mathrm{loc},i}$ are known, $I^{2\omega}_{J,\mathrm{incoh}}$ and $I^{2\omega}_{J,\mathrm{coh}}$ are obtained from Eqs. (1) and (2) by setting $k=l$ and $k\neq l$, respectively. As discussed in Sec. II, reweighting of liquid configurations is not necessary for $E_Z<10^9$ V/m. Finally, the HRS-depolarization ratios are obtained from $D=I^{2\omega}_{X}/I^{2\omega}_{Z}$ with $I^{2\omega}_{J}=I^{2\omega}_{J,\mathrm{coh}}+I^{2\omega}_{J,\mathrm{incoh}}$ and $D_{\mathrm{incoh}}=I^{2\omega}_{X,\mathrm{incoh}}/I^{2\omega}_{Z,\mathrm{incoh}}$. All results are displayed in Table II. The table also shows the linear counterparts of the scattering intensities, $I^{\omega}_{J,\mathrm{coh}}$ and $I^{\omega}_{J,\mathrm{incoh}}$, and depolarization ratios, $\Delta=(I^{\omega}_{X,\mathrm{coh}}+I^{\omega}_{X,\mathrm{incoh}})/(I^{\omega}_{Z,\mathrm{coh}}+I^{\omega}_{Z,\mathrm{incoh}})$ and $\Delta_{\mathrm{incoh}}=I^{\omega}_{X,\mathrm{incoh}}/I^{\omega}_{Z,\mathrm{incoh}}$. [The $I^{\omega}_{J,\mathrm{incoh}}$ are obtained from an expression analogous to Eq. (2) with $\mu_{\beta,kJ}$ replaced by $\mu_{\alpha,kJ}$, the $\alpha$ indicating that $\underline{\underline{\alpha}}\cdot\underline{E}_{\mathrm{loc},i}$, instead of $\underline{\underline{\beta}}:\underline{E}\underline{E}_{\mathrm{loc},i}$, is needed in Eq. (2)].

The $\Delta_{\mathrm{incoh}}$ and $D_{\mathrm{incoh}}$ extracted from the simulation may be compared to the depolarization ratios calculated when assuming independent scatterers that are all subject to the same external fields.[19] The incoherent linear depolarization ratio calculated from such an approach is given by

$$\Delta_{\mathrm{incoh}}=\frac{\langle\alpha^2_{XY}\rangle}{\langle\alpha^2_{ZZ}\rangle}=\frac{A-B}{3A+2B} \tag{5}$$

with $A=1/15\Sigma_i\alpha_{ii}$ and $B=1/15\Sigma_{i<j}\alpha_{ii}\alpha_{jj}$, and the brackets denote orientational averaging of the scatterer with respect to the laboratory coordinate frame.[9] The incoherent HRS-depolarization ratio obtained from this approach is given by[5–7]

$$D_{\mathrm{incoh}}=\frac{\langle\beta^2_{XZZ}\rangle}{\langle\beta^2_{ZZZ}\rangle} \tag{6}$$

[the actual averaging of the quantities on the right-hand side of Eq. (6) is explained in Appendix B of Ref. 7]. The $\Delta_{\mathrm{incoh}}$ and $D_{\mathrm{incoh}}$ obtained from Eqs. (5) and (6) are also shown in Table II. Clearly, the comparison with the simulated depolarization ratios is excellent. This does not necessarily mean that the values of $\Delta_{\mathrm{incoh}}$ and $D_{\mathrm{incoh}}$ are of high quality (this is solely determined by the quality of the $\alpha_{ij}$'s and $\beta_{ijk}$'s); it only indicates that our simulation is long enough to achieve proper orientational averaging of the scatterers.

Our main interest in the data of Table II is as follows. From the Rayleigh scattering data it is clear that $\Delta_{\mathrm{incoh}}$, a quantity which would be obtained from an experiment on a dilute gas, differs from $\Delta$, which would be measured in an experiment on a liquid, by an order of magnitude. This huge difference is caused by the fact that generally for Rayleigh scattering,[7] $I^{\omega}_{J,\mathrm{coh}}\gg I^{\omega}_{J,\mathrm{incoh}}$, because the generation of coherent Rayleigh scattering only requires density fluctuations. Since these extend over length scales that are large compared to the dimensions of a molecule [see Fig. 2 for a picture of $g(r)$], a relatively large fraction of the total radiation is of coherent intermolecular origin.

The hyper-Rayleigh scattering data presented in Table II show a different picture. For this type of scattering, we find that $I^{2\omega}_{J,\mathrm{coh}}\approx I^{2\omega}_{J,\mathrm{incoh}}$ and $D_{\mathrm{incoh}}\approx D$. The reason that $I^{2\omega}_{J,\mathrm{coh}}$ has now become much less important is that for HRS both density and orientational fluctuations that create locally a noncentrosymmetric structure, have to be present. Since these necessarily extend over distances smaller than spatial density fluctuations alone, the relative amount of coherent radiation that is generated is much less than in a Rayleigh scattering experiment. As an illustration of this notion, focus on the (nearly) antiparallel dimerization that occurs in the nitrobenzene liquid (see Sec. III and Refs. 33 and 34). It is clearly seen from Fig. 2 that this dimerization causes an extra peak and valley pattern in $g(r)$, and thus increases the spatial fluctuations in the nitrobenzene liquid. However, locally, i.e., on Å length scales, the antiparallel dipolar ordering tends to create a (nearly) centrosymmetric dimeric structure (see Figs. 3 and 4). As a result, despite the presence of density fluctuations, the dimerization process is expected to contribute very little to the coherent HRS signal, since contributions can only be expected from imperfectly aligned dimers.

Although the generation of coherent radiation is much less important in HRS than in Rayleigh scattering, our results clearly indicate that about half of the HRS radiation is of

coherent origin. Interpretations of the HRS signal in terms of incoherent radiation alone should therefore be mistrusted (despite the fact that $D \approx D_{\text{incoh}}$; we regard this as merely fortuitous). It seems safer when experimenting on pure liquids, to estimate what fraction of the HRS signal has a coherent origin (e.g., via an approach of the type present here), instead of directly assuming $D_{\text{incoh}}$ in order to use Eq. (6) to calculate the molecular tensor elements $\beta_{ijk}$. Another option practiced by many experimentalists[3–5] is to work with dilute solutions whenever possible: We estimate that using solvents with first hyperpolarizabilities that are smaller by an order of magnitude than the first hyperpolarizability of the solute of interest is sufficient to mainly generate incoherent radiation. For pure liquid nitrobenzene we have established that $\langle \Sigma_k \mu^2_{\beta,kJ} \rangle \approx \langle \Sigma\Sigma_{k\neq l} \mu_{\beta,kJ} \mu_{\beta,lJ} \rangle$, therefore it can be anticipated that in dilute solutions when $\beta_{\text{solute}} \approx 10\beta_{\text{solvent}}$, $\langle \Sigma_k \mu^2_{\beta,kJ} \rangle \approx 10 \langle \Sigma\Sigma_{k\neq l} \mu_{\beta,kJ} \mu_{\beta,lJ} \rangle$ ($k$ is solute, $l$ is solvent). Thus, in such dilute solutions we have $I^{2\omega}_{J,\text{incoh}} \approx 10 I^{2\omega}_{J,\text{coh}}$, allowing interpretation in terms of incoherent radiation only.

In view of the considerable uncertainty associated with experimental values of $\beta$ reported in the literature, we have performed an elementary sensitivity analysis to assess changes in the calculated depolarization ratio brought about by changes in the $\beta$ value input to the calculation: We have rerun the electrostatics with the $\beta_{zzz}$ component of the first hyperpolarizability tensor increased by 40%, leaving the other tensor elements unchanged. Increasing the hyperpolarizability gave $D_{\text{incoh}} = 0.26$ [Eq. (6) gives 0.255] and $D = 0.27$. Therefore, we expect an actual experiment to produce a value in the range $D = 0.27 - 0.29$.

The closest experiment[5] that we can compare our $D$ to is on paranitroaniline (pNA), which has an extra $NH_2$ group in the *p* position. From these experiments on a dilute solution of pNA in methanol and chloroform, the $D_{\text{incoh}}$ of pNA was estimated to be 0.23. This value is much lower than predicted by our simulation on liquid nitrobenzene, which is in agreement[7] with the significant enhancement of the $\beta_{zzz}$ value of pNA when compared to the nitrobenzene molecule (roughly by an order of magnitude). Nevertheless, in order to say anything more conclusive, it seems necessary to verify our results experimentally. This may be possible by studying the HRS signal of a series of nitrobenzene/benzene mixtures of varying nitrobenzene content. In this way it should also be possible to assess both coherent and incoherent contributions to the HRS signals.

## IV. CONCLUSIONS

MD simulation utilizing an ''*a posteriori*'' applied electric field[12] has been used to obtain the local fields and hyper-Rayleigh scattering depolarization ratio of liquid nitrobenzene from the molecular dipole moment and static ''gas phase'' (hyper)polarizabilities calculated via high quality *ab initio* calculations. In contrast to previous theoretical work, we have quantified both incoherent and coherent scattering arising from the combined appearance of density fluctuations and orientational fluctuations, creating locally a noncentrosymmetric molecular environment. By drawing a parallel to Rayleigh scattering, it was shown that in the case of hyper-Rayleigh scattering, coherent radiation is much less abundant, although non-negligible: It was predicted that for liquid nitrobenzene about half of the HRS is of coherent origin. Therefore, when working with pure liquids, care should be taken in interpreting the HRS experiments in terms of incoherent radiation only. It seems safer to resort to an approach of the type presented here to get insight into the balance between coherent and incoherent HRS. (Note that, due to the absence of angular dependence of the coherent HRS signal, there is no other obvious way of doing this.) Another option is to perform the experiments in a dilute solution. Numerical results obtained from our work indicate that in solvent/solute combinations for which $\beta_{\text{solute}} \approx 10\beta_{\text{solvent}}$, one can safely neglect coherent contributions to the HRS signal. Since working with dilute solutions is already common practice in HRS experiments, our work may be regarded as numerical support justifying the experimental procedures.

Another important result of our work is that we have been able to assess the specifics of the local fields experienced by the nitrobenzene molecules in much greater detail than obtained so far. It is established that the local fields in the liquid are largely determined by ''specific'' dipolar alignment of neighboring nitrobenzene molecules. We believe that developing methods to obtain such specific information on the local fields is of general importance since the local fields may be useful input for *ab initio* quantum chemical work geared at incorporating the molecule's local environment on the values of its dipole moment and (hyper)polarizabilities.

Finally, in future efforts, we intend to extend our work to substances with stronger polarity and nonlinearities (e.g., water) and to materials that are of technological relevance (e.g., polythiophenes).

## ACKNOWLEDGMENT

We gratefully acknowledge support from the European Commission in the form of a TMR Network Grant (Contract No. ERB-FMRX-CT96-0047).

[1] P. N. Prasad and D. J. Williams, *Introduction to Nonlinear Optical Effects in Molecules and Polymers* (Wiley-Interscience, New York, 1991).
[2] E. G. J. Staring, Recl. Trav. Chim. Pays-Bas **110**, 492 (1991).
[3] K. Clays and A. Persoons, Phys. Rev. Lett. **66**, 2980 (1991).
[4] K. Clays and A. Persoons, Rev. Sci. Instrum. **63**, 3285 (1992).
[5] G. J. T. Heesink, A. G. T. Ruiter, N. F. van Hulst, and B. Bölger, Phys. Rev. Lett. **71**, 999 (1993).
[6] M. Kauranen and A. Persoons, J. Chem. Phys. **104**, 3445 (1996).
[7] R. Bersohn, Y.-H. Pao, and H. L. Frisch, J. Chem. Phys. **45**, 3184 (1966).
[8] R. W. Terhune, P. D. Maker, and C. M. Savage, Phys. Rev. Lett. **14**, 681 (1965).
[9] D. A. McQuarrie, *Statistical Mechanics* (Harper and Row, New York, 1976).
[10] T. Keyes, and B. M. Ladanyi, in *Advances in Chemical Physics*, Vol. LVI, 411 (Wiley, New York, 1984).
[11] J. O. Hirschfelder, C. F. Curtiss, and R. B. Bird, *Molecular Theory of Gases and Liquids* (Wiley, New York, 1964).
[12] R. H. C. Janssen, J. M. Bomont, D. N. Theodorou, S. Raptis, and M. G. Papadopoulos, J. Chem. Phys. **110**, 6463 (1999).
[13] J. A. Armstrong, N. Bloembergen, J. Ducuing, and P. S. Pershan, Phys. Rev. **127**, 1918 (1962).

[14] R. P. Feynman, *The Feynman Lectures on Physics* (Addison-Wesley, Reading, MA, 1964), Vol. 2.
[15] D. Frenkel and J. P. McTague, J. Chem. Phys. **72**, 2801 (1980).
[16] B. M. Ladanyi, J. Chem. Phys. **78**, 2189 (1983).
[17] D. Frenkel and B. Smit, *Understanding Molecular Simulation* (Academic, London, 1996).
[18] D. J. Adams and I. R. McDonald, Mol. Phys. **32**, 4 (1962).
[19] H. C. van de Hulst, *Light Scattering by Small Particles* (Wiley, New York, 1957),
[20] R. Edberg, D. J. Evans, and G. P. Morriss, J. Chem. Phys. **84**, 6933 (1986).
[21] G. Ciccotti, M. Ferrario, and J. P. Ryckaert, Mol. Phys. **47**, 1253 (1982).
[22] M. P. Allen and D. J. Tildesley, *Computer Simulation of Liquids* (Oxford Science, Oxford, 1987).
[23] R. W. Munn, Mol. Phys. **64**, 1 (1988).
[24] C. J. F. Böttcher, *Theory of Electric Polarization* (Elsevier, Amsterdam, 1952).
[25] V. A. Shlyapochnikov, L. S. Khaikin, O. E. Grinka, C. W. Bock, and L. V. Vilkov, J. Mol. Struct. **326**, 1 (1994).
[26] *Handbook of Chemistry and Physics*, edited by R. C. Weast (CRC, Boca Raton, FL, 1988).
[27] M. W. Schmidt, K. K. Baldridge, J. A. Boatz, S. T. Elbert, M. S. Gordon, J. H. Jensen, S. Kozeki, M. Matsunaga, K. A. Nguyen, S. J. Su, T. L. Windus, M. Dupuis, and J. A. Montgomery, J. Comput. Chem. **143**, 1347 (1993).
[28] A. J. Sadlej, Coll. Czech. Chem. Commun. **53**, 1995 (1988).
[29] J. A. Pople, J. S. Binkley, and R. Seeger, Int. J. Quantum Chem., Quantum Chem. Symp. **10**, 1 (1976).
[30] (a) W. J. Hehre, R. Ditchfield, and J. A. Pople, J. Chem. Phys. **56**, 2257 (1972). (b) R. Ditchfield, W. J. Hehre, and J. A. Pople, J. Chem. Phys. **54**, 724 (1971). (c) P. C. Hariharan and J. A. Pople, Theor. Chim. Acta **28**, 213 (1973).
[31] K. D. Singer and A. F. Garito, J. Chem. Phys. **75**, 3572 (1981).
[32] B. F. Levine and C. G. Bethea, J. Chem. Phys. **63**, 2666 (1975).
[33] A. Piekara and A. Chelkowski, J. Chem. Phys. **25**, 794 (1956).
[34] A. Piekara, Proc. R. Soc. London, Ser. A **172**, 360 (1939).
[35] T. K. Sherwood, R. L. Pigford, and C. R. Wilke, *Mass Transfer* (McGraw-Hill, New York, 1975).